Available online at www.sciencedirect.com
SCIENCE DIRECT
Catalysis Today 107–108 (2005) 133–138
CATALYSIS TODAY
www.elsevier.com/locate/cattod

# A theoretical and experimental study of manganese oxides used as catalysts for VOCs emission reduction

Luciano Lamaita [a], M. Andrés Peluso [a], Jorge E. Sambeth [a,*], Horacio Thomas [a], Giuliano Mineli [b], Piero Porta [b]

[a] *Centro de Investigación y Desarrollo en Ciencias Aplicadas "Dr. Jorge J. Ronco", CINDECA (UNLP-CONICET), 47 Nr. 257, B1900AJK La Plata, Argentina*
[b] *Dipartimento di Chimica, Universitádegli studi di Roma "La Sapienza", Roma, Italy*

Available online 26 August 2005

**Abstract**

Complete oxidation of ethanol, as model volatile organic compound, was investigated on manganese oxides catalysts.

The catalysts were prepared by two different methods: (1) oxidative decomposition of $MnCO_3$ under flowing oxygen saturated with water and (2) oxidation of a $MnSO_4$ dissolved in $H_2SO_4$. The solids were characterized by XRD, diffuse reflectance IR spectroscopy (DRIFTS), DRS–UV–vis and thermogravimetric analyses (TGA). The results showed that both solids belonged to the nsutite phase ($\gamma$-$MnO_2$). Both catalysts showed similar catalytic activity in the complete oxidation of ethanol. The maximum activity of the catalysts was related to the structure of the catalysts ($Mn^{4+}$ vacancies, presence of $Mn^{3+}$ ions and OH groups). The catalyst obtained by decomposition of $MnCO_3$ is the best catalyst because it is easier to prepare. The theoretical results revealed two possible adsorption–oxidation sites of $C_2H_5OH$ on the nsutite phase; the OH groups formed from $Mn^{4+}$ vacancies, where ethanol could be oxidized to $CO_2$ and the terminal oxygen of the pyrolusite lattice, where ethanol could be partially oxidized to acetaldehyde, which it could be oxidized to $CO_2$.


*Keywords:* Manganese oxides; Nsutite; DRIFTS; VOCs; Extended Hückel method (EHMO)-ASED

## 1. Introduction

Manganese oxides ($MnO_2$, $Mn_2O_3$ and $Mn_3O_4$) have been reported in some environmental catalysis reactions such as the selective reduction of $NO_x$ and CO, oxidation of VOCs, total oxidation of methane and elimination of organoclorates [1–7].

There are many $MnO_2$ polymorphs. The tetragonal pyrolusite ($\beta$-$MnO_2$) and the orthorhombic ramsdellite are two of them. These form a three dimensional network of edge and corner-sharing $MnO_6$ octahedral arranged in simple chains (pyrolusite) and double chains (ramsdellite, R-$MnO_2$) [8]. The nsutite ($\gamma$-$MnO_2$) is formed by the intergrowth of domains of pyrolusite and ramsdellite and $\gamma$-$MnO_2$ is used as cathode material for dry cell. Chabre and Pannetier [8] have reported about 14 $\gamma$-$MnO_2$ modifications. This solid is characterized by three types of defects: (a) De Wolff disorder—the intergrowth of ramsdellite and pyrolusite, (b) micro twinning and (c) point defects such as $Mn^{4+}$ vacancies and $Mn^{3+}$ cations. They have shown that micro twinning and De Wolff disorder are responsible for a poor crystalline structure and the $\gamma$-$MnO_2$ electrochemical properties.

MacLean et al. [9] and Ruestchi and Giovanoli [10] have demonstrated that the structural and chemical defects are responsible for the electrochemical properties by the $H^+$ insertion and increasing the Fermi level energy. According to Volkshtein Electronic Theory [11], these properties make these oxides interesting, from the catalytic point of view, due to their high electrical conductivity.

Provided the catalytic interest in these phases of Mn as destruction of VOC's, our objective in this work is: (1) to obtain $\gamma$-$MnO_2$ by different methods, (2) to study the

* Corresponding author. Tel.: +54 221 4211353; fax: +54 221 4214277.
*E-mail address:* sambeth@quimica.unlp.edu.ar (J.E. Sambeth).

0920-5861/$ – see front matter © 2005 Elsevier B.V. All rights reserved.
doi:10.1016/j.cattod.2005.07.155

catalytic activity in the complete oxidation of ethanol and (3) to study theoretically the adsorption–oxidation process on different sites.

## 2. Experimental

### 2.1. Samples preparation

Two manganese oxides were prepared by different methods in order to obtain the nsutite or γ-$MnO_2$ phase.

One of them was obtained by oxidative decomposition of $MnCO_3$ (Riedel de Haen RG) at 350 °C under flowing oxygen saturated with water (50 $cm^3$ $min^{-1}$) for 1 h, and with a heat rate of 20 °C $min^{-1}$. This oxide is named hereinafter M1.

The other manganese oxide (M2) was synthesized by oxidation with flowing oxygen (30 $cm^3$ $min^{-1}$) of a $MnSO_4$ dissolved in 3 M $H_2SO_4$. pH was raised up to 3 with NaOH. After being filtered and washed with deionized water, the oxide was dried at 100 °C for 24 h [12].

These oxides were compared with a commercial $MnO_2$ (Baker 99%) and with a synthetic $Mn_2O_3$ obtained by decomposition of $MnCO_3$ [3].

### 2.2. Characterization

X-ray diffraction patterns were carried out at room temperature with a Phillips PW 1390 instrument by using Ni filter and Cu Kα radiation (λ = 1.540589 Å) in the 2$\theta$ range between 5 and 60°. For phase identification purposes, JCPDS database of reference compounds was used [13].

DRIFTS spectra were obtained in a Bruker IFS66 infrared spectrometer with a KBr optics and DTGS detector in the 600–4000 $cm^{-1}$ range. The spectra were obtained by co-adding 200 scans collected at 4 $cm^{-1}$.

DRS–UV–vis spectra were recorded on a Cary 2300 spectrophotometer in the 200–2000 nm region.

Thermal analyses of small sample portions of the samples (16 mg) were carried out on a DTA-TG 50 Shimadzu analyzer, between room temperature and 900 °C; at 10 °C $min^{-1}$ in a flowing air atmosphere (30 $cm^3$ $min^{-1}$).

### 2.3. Catalytic activity

The ethanol combustion reaction was carried out at atmospheric pressure in a continuous flow tubular glass reactor filled with 0.200 g of catalysts. An air stream saturated with ethanol was created by using a saturator equipped with temperature and pressure controls, and then diluted with pure air resulting in a 300 ppm ethanol concentration in the reactor feed. The total gas flow was 20 $cm^3$ $min^{-1}$.

The reactants and reaction products were analyzed using on-line gas chromatograph (Shimadzu GC 8A) equipped with thermal conductivity detector. The analysis of ethanol, acetaldehyde and $CO_2$ was conducted through a Porapack T column.

### 2.4. Theoretical method

Extended Hückel Method (EHMO-ASED) is an acceptable approach to the electronic structure of a solid when transition metals are involved. Although the method does not give absolute representative results, it predicts well the relative trends defined by a simple calculation procedure [14]. The relative energy of the system ($E_r$), includes terms for both repulsion and binding energies and the $H_{ii}$ parameter and coefficients ($\xi$) used for the calculations are indicated in Table 1 [15]. The Wolfsberg–Helhmotz constant employed was 1.70.

To represent nsutite structures the MOLMOD program was used. We used the atomic distances of $MnO_6$ octahedra reported by Bystrom [16]. Once the octahedral was obtained, the structures of pyrolusite and ramsdellite were configured, in accordance with the data reported by Potter and Rossman [17].

Nsutite structure was studied by calculating the minimum relative system energy of the system ($E_r$). Nsutite structure was built up from pyrolusite elements interspersed in a ramsdellite matrix. Once the nsutite energy minimum was determined, we introduced one $Mn^{4+}$ vacancy into a ramsdellite or pyrolusite cell. For charge compensation, protons that made four of the six oxygen anions surrounding the vacancy $OH^-$ anions were used.

For $C_2H_4OH$ molecule, gaseous bond length and angles were employed [18]. The adsorption–oxidation process was studied on the basis of calculations of the total system energy. This energy ($E_r$) was calculated as the difference between the system energy when the molecule is at a finite distance from the surface and the energy at infinite distance.

## 3. Results and discussion

Data from XRD indicated the presence of β-$MnO_2$ or pyrolusite phase (JCPDS 24-0735) for the commercial manganese dioxide and a well crystallized α-$Mn_2O_3$ (JCPDS 41-1442) for the synthesized $Mn_2O_3$.

Table 1
Tables of parameters for Extended Hückel Method-ASED [15]

| Atom | Orbital | $H_{ii}$ (eV) | $\zeta_{i1}$ | $C_1$ | $\zeta_{i2}$ | $C_2$ |
|---|---|---|---|---|---|---|
| Mn | 4s | −9.75 | 0.97 | | | |
| | 4p | −5.89 | 0.97 | | | |
| | 3d | −11.67 | 5.15 | 0.5139 | 1.70 | 0.6929 |
| O | 2s | −32.3 | 2.275 | | | |
| | 2p | −14.8 | 2.275 | | | |
| H | 1s | −13.6 | 1.30 | | | |
| C | 2s | −21.4 | 1.625 | | | |
| | 2p | −11.4 | 1.625 | | | |

Fig. 1 shows the XRD powder patterns of both synthesized manganese samples. Neither $MnCO_3$ nor $MnSO_4$ is present in M1 and M2 samples, respectively, and it can be seen that both oxides present a nearly amorphous X-ray powder diffraction pattern, in accordance with Chabre and Pannetier [8], who have reported that gamma manganese dioxides generally show poorly resolved XRD patterns. Nevertheless, some peaks are detected, such as 37°, 42° and 56° in M1 and 22°, 37°, 38°, 42° and 56° in M2. The XRD patterns of M2 account for a γ-$MnO_2$ phase (JCPDS 17-0510). In the case of the former, it is similar to M2, except for the missing peaks at 22 and 38°, and it could be a γ-$MnO_2$ with more chemical defects [8]. On the other hand, no crystalline $Mn_2O_3$ is observed in these two samples.

The DRIFTS spectra are shown in Fig. 2. No peaks of $Mn_2O_3$ are detected in the samples [3]. The positions of the bands in M1 and M2 are coincident with that reported by Potter and Rossman [17] for the γ-$MnO_2$ phase, which is in agreement with the XRD data. These authors have reported that ramsdellite presents peaks at 522, 630, 649 and 743 $cm^{-1}$. As we mentioned in the introduction, $MnO_2$ exists in various polymorphous modifications, so they are usually represented by $T(n,m)$ where $n$ and $m$ stand for the dimensions of the tunnels in the two directions perpendicular to the chains of edge-sharing octahedral. In this representation, pyrolusite and ramsdellite are symbolized by $T(1,1)$ and $T(1,2)$, respectively. Nsutite or γ-$MnO_2$ could be described as an irregular intergrowth of elements of ramsdellite and pyrolusite, so that the representation would be $T(1,1)$–$T(1,2)$. It is possible to obtain the structural characteristics of the manganese dioxides taking into account the correlation of infrared spectra made by Potter and Rossman [17], who pointed out that IR bands shifted to a lower wave number with increasing octahedral polymerization. This trend can be observed in Fig. 3, where it was plotted the frequency position of the infrared active modes of our oxides as a function of the average $MnO_6$ octahedral

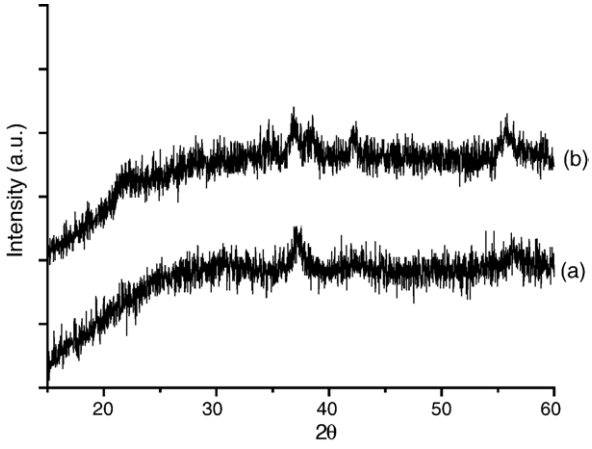


Fig. 1. X-ray powder diffraction patterns of the manganese oxides: (a) M1 and (b) M2.

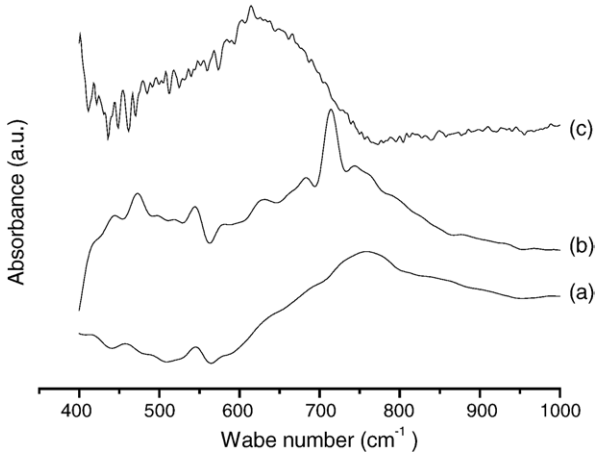


Fig. 2. DRIFTS spectra of manganese oxides samples: (a) M1, (b) M2 and (c) β-$MnO_2$.

polymerization. It is clearly observed that the IR bands of M1 and M2 are between the bands of pyrolusite and ramsdellite. This means that both samples consist of a distribution of pyrolusite and ramsdellite, in good agreement with de Wolff [19], Norman et al. [20] and Shaheen and Selim [21] results.

The presence of $Mn^{3+}$ and $Mn^{4+}$ cations was determined by DRS–UV–vis. Fig. 4 shows the positions of the UV bands for the synthesized catalysts and the references. M1 and M2 present absorption at approximately 340 nm and in the 450–550 nm regions. The former absorption is also present in pyrolusite, where the Mn is present in the 4+ valence, and is associated to $Mn^{4+}$ [22]. The latter, which is present in $Mn_2O_3$, is attributed to $O^{2-}$–$Mn^{3+}$ charge transfer [23]. In conclusion, both M1 and M2 samples present $Mn^{3+}$ and $Mn^{4+}$ in their structures.

According to Ruestchi and Giovanoli [10], the presence of structural water influences electrochemical reactivity,

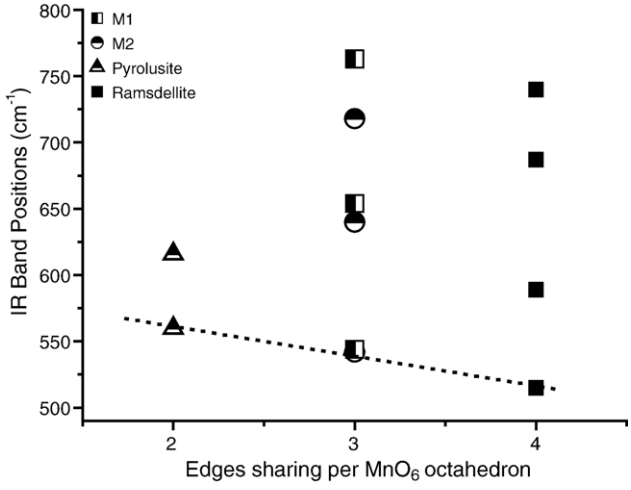


Fig. 3. Frequency positions of the IR bands as function of the average $MnO_6$ octahedral polymerization in manganese oxides. (ramsdellite bands, Potter and Rosmann [17]).

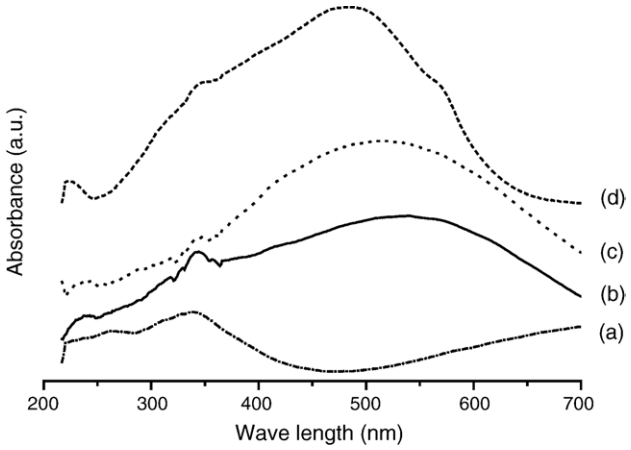


Fig. 4. DRS–UV–vis spectra of manganese oxides samples: (a) β-$MnO_2$, (b) M2, (c) M1 and (d) $Mn_2O_3$.

density and electronic conductivity. Fig. 5 shows the weight loss in percentage in each sample. The transformation of $MnO_2$ to $Mn_2O_3$ starts at a higher temperature for pyrolusite than for the other oxides. This indicated that this oxide is possibly less active than the others, as reported by González et al. [24]. The transformation to $Mn_2O_3$ in M1 sample occurs at 585 °C. It can be seen that M2 sample is still losing weight at 800 °C. Petit et al. [25] have shown that γ-$MnO_2$ is non-stoichiometric unless the temperature is increased up to 800 °C, because there are OH groups in the bulk of the material, and it is electrochemically active up to 450 °C. These phenomena make this oxide very interesting for catalytic purposes, due to the high temperature at which it is non-stoichiometric.

So far the characterization results have shown that M1 and M2 samples: (i) are members of the nsutite or γ-$MnO_2$ family, constituted by an intergrowth of pyrolusite and ramsdellite, (ii) contain $Mn^{3+}$ ions in their structure, which are related to the presence of OH groups but they are not present in the form of crystalline $Mn_2O_3$, (iii) they present different behaviors at high temperature by thermal treatment, nevertheless at low temperature, up to 400 °C their behaviors are similar and (iv) they have OH groups not only on the surface but also in the inner part of the tunnels and they are stable at high temperatures. These characteristics are in agreement with the postulated Volkenshtein Electronic Theory [11], which pointed out that the formation of vacancies and defects modifies the Fermi Energy level and favors the catalytic reactions.

The catalysts were tested in the reaction of complete oxidation of ethanol according to the experimental procedure above described. Carbon dioxide, water and acetaldehyde were the reaction products. Results of ethanol conversion as a function of the reaction temperature for the manganese oxide catalysts are shown in Fig. 6. The results with $Mn_2O_3$ as catalyst (which have been reported in a previous paper [3]) are included for comparison. It can be seen that both M1 and M2 samples have a similar activity, characterized by a $T_{50}$ (temperature at which the conversion is 50%) of approximately 150 °C. For both catalysts the conversion reaches 100% below 200 °C, with selectivity to $CO_2$ of 100%. Acetaldehyde is found at low conversion values, between 100 and 150 °C. Commercial manganese dioxide, (β-$MnO_2$), and $Mn_2O_3$ have a $T_{50}$ of 250 and 180 °C, respectively, and conversion reaches 100% above 300 and 230 °C, respectively. Taking into account the characterization results and the works of Peluso et al. [3], Shaheen and Selim [21] Radwan [26], Hill et al. [27] and the studies of Chabre and Pannetier [8] about the correlation between the electrochemical properties and the crystallinity, we can say that the high activity of M1 and M2 samples could be explained by: (i) the existence of the $Mn^{3+}$–$Mn^{4+}$ couple, (ii) the poor crystallinity of the oxides and (iii) the $Mn^{4+}$ vacancies, which generate OH groups (associated with loss of water) and are still present at 200 °C when the conversion is 100%.

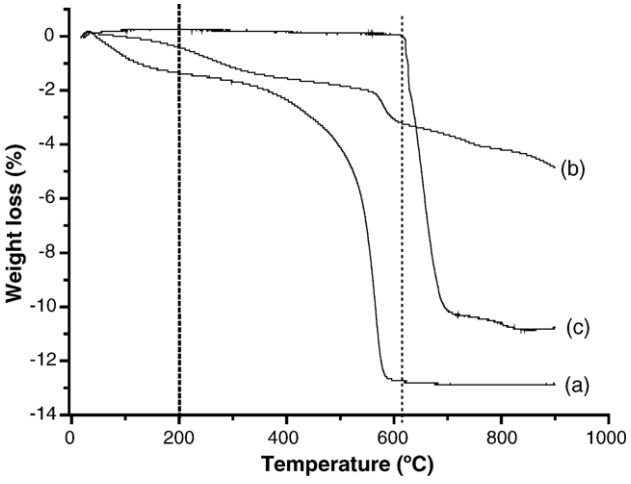


Fig. 5. TGA curves for manganese oxides: (a) M1, (b) M2 and (c) β-$MnO_2$.

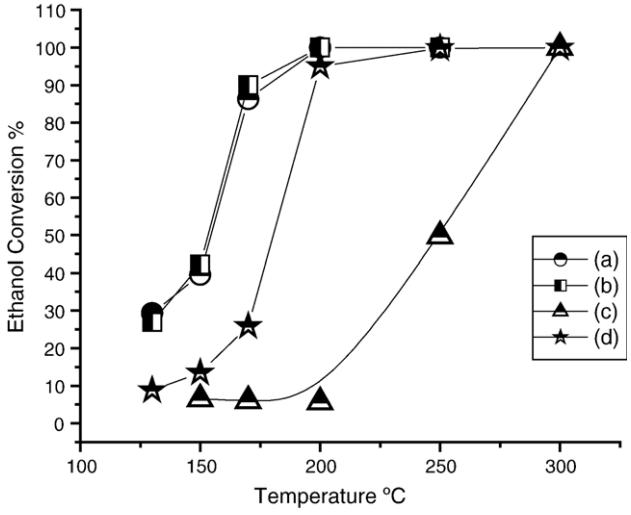


Fig. 6. Total ethanol conversion as a function of temperature: (a) M1, (b) M2, (c) $Mn_2O_3$ and (d) β-$MnO_2$.

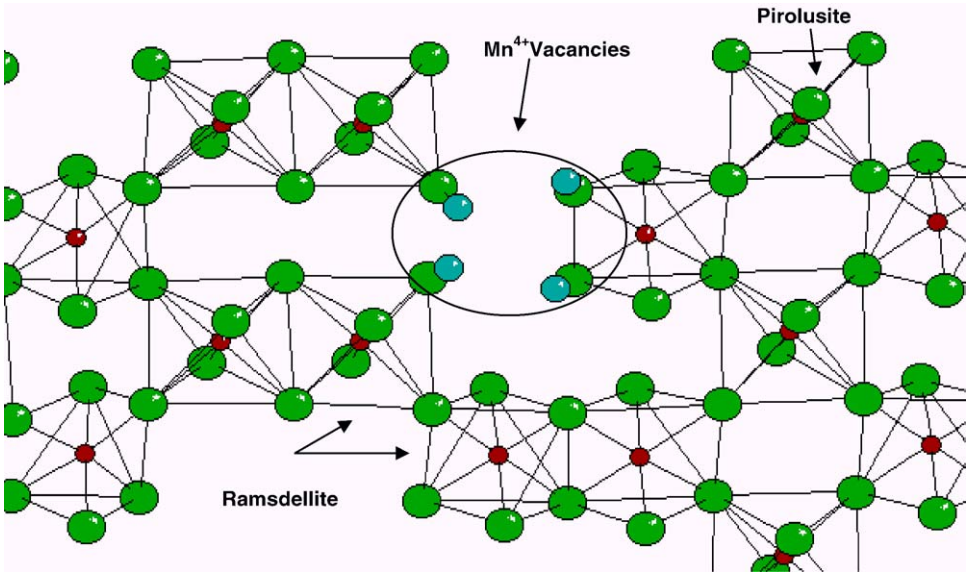


Fig. 7. Geometric structure of the nsutite ($\gamma$-$MnO_2$). One manganese vacancy was placed on the ramsdellite octahedron.

The theoretical calculation by EHMO was carried out by analyzing the most energetically favorable positions of the $H^+$. The results show that the protons with the highest stability were those localized over the oxygen in Mn vacancies generated in ramsdellite octahedrons (see Fig. 7). These results are in agreement with that reported by Ruestchi and Giovanoli [10] who have proposed that the predominant protons sites are the oxygen atoms surrounding the Mn vacancies in ramsdellite.

Because $CO_2$ and acetaldehyde were found in the reaction products, we analyzed on the one hand the oxidation of ethanol to $CO_2$ and on the other the oxidation of ethanol to acetaldehyde. For this purpose, once the lattice was built and the protons were placed, we studied the adsorption of ethanol over three different positions (see Fig. 8). The first studied site (site 1, Fig. 8) was represented by $CH_3CH_2OH$ adsorption from the gaseous phase, which involves an H of the OH group of the alcohol with an O of the ramsdellite lattice. This interaction turns the energy ($E_r$) of the system into −3249 eV. The second position (site 2, Fig. 8) studied involved similar interaction but with an O of the pyrolusite lattice. The relative energy ($E_r$) of this interaction was −3335 eV. In the third position (site 3, Fig. 8), we studied the interaction between the O of the ethanol OH group with an $H^+$ of the nsutite lattice. This interaction was the most energetically favorable with a relative energy ($E_r$) value of −3365 eV. Taking into account the bond distances, we rotated the adsorbed ethanol molecule over the third position under study. We found the minimum energy of the system ($E_r$ = −3407 eV)

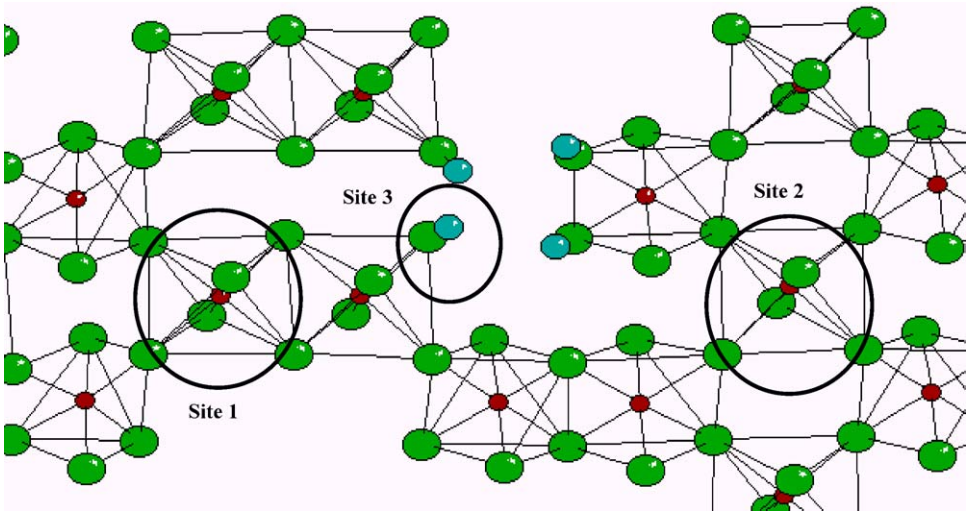


Fig. 8. Representation of the different sites for ethanol oxidation (see text).

when the C of the $CH_3$ group interacted with an O of the lattice and an H of the $CH_2$ group interacted with another O of the lattice. The structure of this adsorbed species led to the formation of a carboxylate group. These results are in agreement with Finocchio and Busca [28] and Peluso et al. [3] who have obtained experimental evidence of the presence of these carboxylate groups in their studies of adsorbed alcohols over manganese oxides.

Batiot and Donet [29] and Blausim-Aubé et al. [30] have demonstrated that the ethanol → acetaldehyde → $CO_2$ mechanism is more favorable than the ethanol → $CO_2$ oxidation. Their conclusions and our results allow us to suggest that the interaction in the site 3 could lead to the formation of an alcoxide specie strongly adsorbed over the lattice, and this could be the place where ethanol oxidizes directly to $CO_2$ at temperatures above the $T_{50}$. Whereas the interaction in the site 2 could lead to the formation of acetaldehyde, which it easily oxidizes to $CO_2$.

## 4. Conclusions

Two nsutite-like oxides were synthesized by different methods. The X-ray diffraction patterns, DRIFTS and DRS–UV–vis demonstrated that both oxides: (i) were nearly amorphous, (ii) presented IR bands associated with the γ-$MnO_2$ phase and (iii) contain $Mn^{3+}$ and $Mn^{4+}$ in their structures, although no $Mn_2O_3$ was detected in either sample. These samples retained OH species at 200 °C when the conversion was total, as it was demonstrated by TG analyses. These materials were active in the ethanol combustion in the 100–200 °C temperature range. They showed almost the same activity and were more active than $Mn_2O_3$ and β-$MnO_2$.

Taking into account that $Mn_2O_3$ and β-$MnO_2$ have a good crystalline structure and are stoichometric oxides, the high activity of our synthesized oxides could be explained by the poor crystallinity of the samples, the presence of the $Mn^{3+}$–$Mn^{4+}$ couple, and the existence of $Mn^{4+}$ vacancies, which generates OH species. EHMO calculations allow us to conclude that there are two different sites for the adsorption and oxidation of ethanol. On one site the alcohol is strongly attached and there could be where ethanol is oxidized directly to $CO_2$ at temperatures above the $T_{50}$.

Finally, although both catalysts have shown the same performance for ethanol oxidation, M1 sample can be obtained in a more simple way and then it is easier to prepare.

## Acknowledgement

The authors express their thanks to UNLP and CONICET for financial support and one of them (MAP) to Comisión de Investigaciones Científicas (CICPBA) for his Ph.D. fellowship.

## References

[1] M. Paulis, L. Ganda, A. Gil, J. Sambeth, J. Odriozola, M. Montes, Appl. Catal. B 26 (2000) 37.
[2] V. Bentrup, A. Bruickner, M. Ritcher, R. Fricke, Appl. Catal B 32 (2001) 229.
[3] M. Peluso, J. Sambeth, H. Thomas, React. Kinec. Catal. Lett. 80 (2003) 241.
[4] M. Álvarez-Galván, V. de la Peña O'Shea, J. Fierro, P. Arias, Cat. Commun. 4 (2003) 223.
[5] L. Gandía, M. Vicente, A. Gil, Appl. Catal. B 38 (2002) 295.
[6] Y. Liu, M. Luo, Z. Wei, Q. Xin, P. Ying, C. Li, Appl. Catal. B 29 (2001) 61.
[7] Y. Liu, Z. Wei, Z. feng, M. Luo, P. Ying, C. Li, J. Catal. 202 (2001) 200.
[8] Y. Chabre, J. Pannetier, Prog. Solid State Chem. 23 (1995) 1.
[9] L. MacLean, C. Poinsignon, J. Amarilla, F. Le Cars, P. Strobel, J. Mater. Chem. 5 (1995) 1183.
[10] P. Ruestchi, R. Giovanoli, J. Electrochem. Soc. 135 (1988) 2663.
[11] F. Volkenshtein, The Electronic Theory of Catalysis on Semiconductors, Pergamon Press, New York, 1963.
[12] S. Netto, R. Hypolito, J. Valarelli, R. Giovanoli, R. Shultz-Gutler, Ann. Acad. Bras. Ci. 70 (3) (1998) 563.
[13] Join Committee on Powder Diffraction Standards, JCPDS Files, International Center for Diffraction Data, 2000.
[14] G. Calzaferri, L. Forss, I. Kamber, J. Phys. Chem. 93 (1998) 5366.
[15] Santiago Alvarez, Universidad de Barcelona, España, Marzo, 1993.
[16] A. Bystrom, Acta Chem. Scand. 3 (1949) 163.
[17] R. Potter, G. Rossman, Am. Mineral. 64 (1979) 1199.
[18] CRC Handbook of Chemistry and Physics, 1982.
[19] P. de Wolff, Acta Cryst. 12 (1959) 341.
[20] A. Norman, M. Kaki, S. Mansour, R. Fahim, C. Kappesntein, Termochim. Acta 210 (1992) 103.
[21] W. Shaheen, M. Selim, Termochim. Acta 332 (1998) 117.
[22] F. Millela, J. Gallardo Amores, M. Balde, G. Busca, J. Mater. Chem. 8 (1998) 2525.
[23] J. Boyero Macstre, E. Fernández López, J. Gallardo Amores, R. Ruano Casero, V. Sanchez Escribano, E. Bernal Pérez, Inorg. Mater. 3 (2001) 889.
[24] C. González, J. Gutierrez, J.G. Velazco, A. Cid, A. Arranz, J. Arranz, J. Termal Análisis 47 (1996) 93.
[25] F. Petit, M. Lenglet, J. Arsene, J. Mater. Res. Bull. 28 (1993) 1093.
[26] N. Radwan, Appl. Catal. A 257 (2004) 177.
[27] J. Hill, C. Freeman, M. Rossouw, J. Solid State Chem. 177 (2004) 165.
[28] E. Finocchio, G. Busca, Catal. Today 70 (2001) 213.
[29] C. Batiot, B. Donet, App. Catal. A 137 (1996) 179.
[30] V. Blausim-Aubé, J. Belkouch, A. Monceaux, Appl. Catal. B 43 (2003) 175.